Article

Not peer-reviewed version

High Repetition-Rate 0.5 Hz Broadband Neutron Source Driven by the Advanced Laser Light Source

Ronan Lelièvre *, Elias Catrix, Simon Vallières, Sylvain Fourmaux, Amokrane Allaoua, Viviange Anthonippillai, Patrizio Antici, Quentin Ducasse, Julien Fuchs

Posted Date: 30 May 2024

doi: 10.20944/preprints202405.2051.v1

Keywords: Neutron; Laser-driven neutron sources, Particle beams; Laser-plasma interactions; High-intensity lasers

Article

High Repetition-Rate 0.5 Hz Broadband Neutron Source Driven by the Advanced Laser Light Source

R. Lelièvre [1,2,*], E. Catrix [3], S. Vallières [3], S. Fourmaux [3], A. Allaoua [2], V. Anthonippillai [1], P. Antici [3], Q. Ducasse [2] and J. Fuchs [1]

[1] LULI - CNRS, CEA, Sorbonne Université, Ecole Polytechnique, Institut Polytechnique de Paris, F-91128 Palaiseau Cedex, France; julien.fuchs@polytechnique.edu (J.F.)
[2] Laboratoire de micro-irradiation, de métrologie et de dosimétrie des neutrons, PSE-Santé/SDOS, IRSN, 13115 Saint-Paul-Lez-Durance, France
[3] INRS-EMT, 1650 Boul. Lionel-Boulet, Varennes, Quebec J3X 1P7, Canada
* Correspondence: ronan.lelievre@polytechnique.edu

Abstract: Neutron beams are an essential tool to investigate material structure and perform non-destructive analysis, as they give unique access to element composition, thus ideally complementing density analysis allowed by standard X-rays investigation. Laser-driven neutron sources, though compact and cost-effective, currently have lower average flux than conventional neutron sources, due to the limited repetition rate of the lasers used so far. However, advancements in laser technology allow nowadays to address this challenge. Here we report results obtained at the Advanced Laser Light Source (ALLS) characterizing stable production of broadband (0.1-2 MeV) neutrons produced at a high repetition rate (0.5 Hz). The interaction of laser pulses of 22 fs duration and 3.2 J on-target energy with 2-μm-thick tantalum targets produced protons in the Target Normal Sheath Acceleration (TNSA) regime up to 7.3 MeV. These protons were subsequently converted into neutrons by (p,n) reactions in Lithium fluoride (LiF). Activation measurements and bubble detectors were used to characterize neutron emissions, with a neutron fluence of up to $\sim 1.4 \times 10^5$ neutrons/shot/sr, and energies mainly between a few hundred of keV and 2 MeV. The total neutron yield was $\sim 5 \times 10^5$ neutrons/shot. This paves the way for numerous applications, e.g. in homeland security, material science or cultural heritage.

Keywords: neutron; laser-driven neutron sources, particle beams; laser-plasma interactions; high-intensity lasers

I. Introduction

Neutrons offer two unique characteristics when used as probes of matter: not only can they penetrate deeper into matter than charged particles (of the same energy), but due to their direct interaction with nuclei they also provide unique insights, through elemental and temperature analysis, of the properties of materials, well beyond the capability of charged particles or X-rays. Laser facilities are now recognized as new particle sources, including the possibility to generate neutron fields [1–4] with very short duration neutron bunches (ps [5] to ns [6]), and record peak brightness [7–10]. These characteristics make laser-driven sources complementary to conventional sources, from very compact, hand-held monochromatic fusion sources [11], to large-ones like fission reactors producing continuous neutrons or accelerators, producing longer neutron pulses (µs at best) [12]. Moreover, the best conventional sources, having a much higher average but lower peak neutron fluxes than the laser-driven sources, have a much larger footprint and cost compared to the latter.

These characteristics are particularly interesting for applications in astrophysics, e.g. by opening up the possibility of characterizing multiple neutron captures [13,14], in non-destructive material analysis for industry [15] or contraband detection [16–18], or for heritage science by performing Neutron Resonance Spectroscopy (NRS) [19,20], or Instrumental Neutron Activation Analysis (INAA) [21], thus complementing Prompt Gamma-ray Activation Analysis (PGAA) [22,23].

However, to improve the prospects of these applications, it is necessary to increase the flux of laser-driven neutron sources by moving to high-repetition rate operation, and to ensure their stability shot after shot. In this work, we present the first measurements of broadband neutron emissions generated repetitively with a laser at a repetition-rate of 0.5 Hz. Note that a recent separate work [24]

 doi:10.20944/preprints202405.2051.v1

has also demonstrated a high-repetition rate (1 kHz) laser-driven neutron source with similar average flux as reported here, but with monochromatic fusion-based neutrons. Here, we used the Advanced Laser Light Source (ALLS), a laser source characterized by a good shot-to-shot laser repeatability [25]. The neutrons were produced by the interaction of protons accelerated from tantalum foils via the Target-Normal Sheath Acceleration (TNSA) mechanism [26–28], and subsequently converted through (p,n) reactions in a LiF converter, in the so-called pitcher-catcher scheme [3].

Section details the experimental setup for performing laser-driven proton acceleration and neutron production. Section shows the results of the experimental characterization of neutron emissions, in comparison with simulations performed using the Monte-Carlo transport codes Geant4 [29] and MCNP6 [30]. Finally, Section delves into the results obtained and provides perspectives induced by this study.

II. Experimental Setup

A. ALLS 150 TW Ti:Sapphire Laser

The experiments were carried out on the laser-driven ion acceleration beamline at the Institut national de la recherche scientifique (INRS) in Varennes, near Montréal, Canada. We used the ALLS 150 TW Ti:Sapphire laser [31] based on a double Chirped Pulse Amplification (CPA) system, delivering 3.2 J on target with a pulse duration of τ_{FWHM} = 22 fs at Full-Width-Half-Maximum (FWHM) and with a central wavelength of λ_0 = 800 nm. The experimental setup, shown in Figure 1.A, uses an $f/3$ off-axis parabola (OAP) to focus the 95 × 95 mm square beam (at e^{-2}) down to a spot size of $w_{\mathrm{FWHM}} \sim 5$ μm. Parabola alignment and wavefront optimization, using a feedback loop between a wavefront sensor and a deformable mirror, are both performed at full laser power, which allows to compensate aberrations arising from thermalization in the laser system. This results in a peak intensity I_0 around 1.3×10^{20} W/cm^2. Prior to entering the second CPA amplification stage, a cross-wave polarizer (XPW) and a booster stage relying on saturable absorber are employed to clean the incoming laser beam, achieving an Amplified Spontaneous Emission (ASE) pre-pulse contrast <10^{-10} at -100 ps before the main pulse, along with a steep power rise with contrast <10^{-6} at -3 ps.

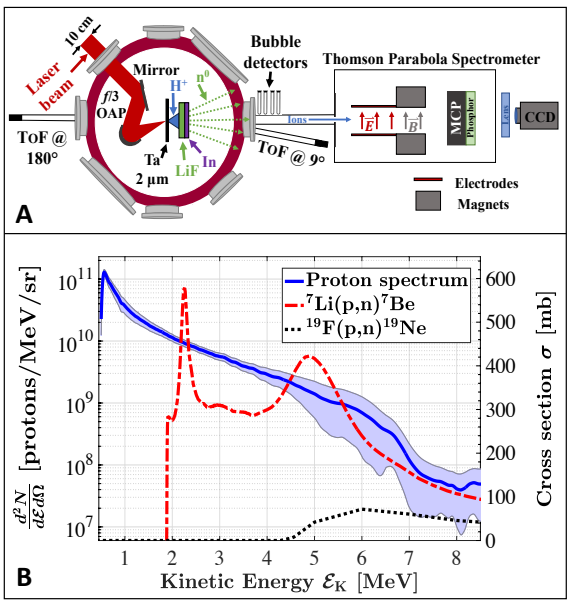

Figure 1. (A) Top-view of the experimental setup for the laser-driven neutron generation. (B) Mean proton spectrum averaged over 38 shots using a 2 μm-thick tantalum foil (full blue). The shaded area is delimited by one standard deviation. The cross sections for the nuclear reactions ^{7}Li(p,n)^{7}Be (dashed red) and ^{19}F(p,n)^{19}Ne (dotted black) are also shown, as given by the ENDF/B-VIII.0 [32] and TENDL-2019 libraries [33], respectively.

 doi:10.20944/preprints202405.2051.v1

B. TNSA-Based Proton Acceleration

The p-polarized laser pulses are incident at an angle of 20° with respect to the target-normal on 2-μm-thick tantalum foils (see Figure1.A) to produce ion beams using the TNSA regime, allowing for 400 consecutive shots by using a custom-made target holder. The experiment is conducted in a 'multi-shot mode' where all target positions are pre-set in the software controlling the motorized stages. The software is synchronized with the laser trigger at 0.5 Hz [25]. The energy distribution of the accelerated ions (mainly protons and carbon ion species) is measured using a calibrated Thomson Parabola (TP) spectrometer positioned at 0° with respect to the target-normal axis, employing a MicroChannel Plate (MCP) detector allowing to acquire the images of the ion spectra for each laser shot. A mean proton spectrum (averaged over 38 shots) is shown on Figure 1.B, characterized by $\sim 10^{11}$ protons/sr/shot and an energy cutoff of 7.3 MeV. Additionally, two Time-of-Flight (ToF) spectrometers are deployed, one positioned at 9° and the other at 180° from the main axis, to monitor the number of protons and their energies in correlation with the TP spectrometer. The latter spectrometer is primarily utilized when the LiF converter is inserted into the ion beam path to verify that the TNSA acceleration occurs efficiently.

C. Neutron Emissions

For the neutron generation, we selected LiF as the converter material in order to maximize the neutron production. Indeed, since the maximum proton cutoff energy is limited to about 7.3 MeV and since the proton spectrum has a typical decreasing exponential shape, LiF is optimum due to its high cross sections of (p,n) reactions for low-energy protons. Further, it has a threshold energy of about 1.9 MeV and a specific resonance at 2.2 MeV of the $^{7}\mathrm{Li}(\mathrm{p},\mathrm{n})^{7}\mathrm{Be}$ reaction (see Figure 1.B). Thus, a 1-mm-thick, 1-inch-diameter LiF converter was placed 20 mm behind the target holder (see Figure 1.A), ensuring that all protons interact with it.

1. Diagnostics

Several techniques were employed to characterize the neutron emissions [34,35], including bubble detectors [36] and activation measurements. Bubble detectors are composed of droplets of a superheated liquid contained in an elastic polymer. These droplets become visible bubbles when neutrons lose their energy inside the detector and, by counting the number of bubbles and considering an appropriate calibration, neutrons doses can be determined. Two types of bubble detectors, supplied by *Bubble Technology Industries*, were used during this experiment: type BD-PND and type BDT. BD-PND detectors are sensitive to neutrons from $\sim$ 200 keV to more than 15 MeV, while BDT detectors are sensitive to thermal neutrons.

An activation diagnostic composed of a 1-inch-diameter and 6-mm-thick pure indium sample, placed right behind the LiF converter (see Figure 1.A), was also used during the experiment. The interaction of neutrons with this sample can cause two main reactions: $^{115}\mathrm{In}(\mathrm{n},\mathrm{n}')^{115\mathrm{m}}\mathrm{In}$ and $^{115}\mathrm{In}(\mathrm{n},\mathrm{fl})^{116\mathrm{m}}\mathrm{In}$. As shown in Figure 2.B, the cross sections of the first reaction are significant between 2 and 10 MeV, allowing to detect neutrons in this energy range, while the second reaction is more sensitive to neutrons from the thermal region to few MeV and serves as a qualitative low-energy neutron diagnostic.

Finally, as the neutrons are produced through the $^{7}\mathrm{Li}(\mathrm{p},\mathrm{n})^{7}\mathrm{Be}$ reaction only (see below), the total number of neutrons can be determined by measuring the $^{7}\mathrm{Be}$ nuclei created in the converter. This radioisotope emits a gamma-ray of 478 keV with an intensity of 10.44% and a half-life time long enough ($\mathrm{T}_{1/2} = 53.22\,\mathrm{d}$) to be easily measured using gamma spectrometry.

 doi:10.20944/preprints202405.2051.v1

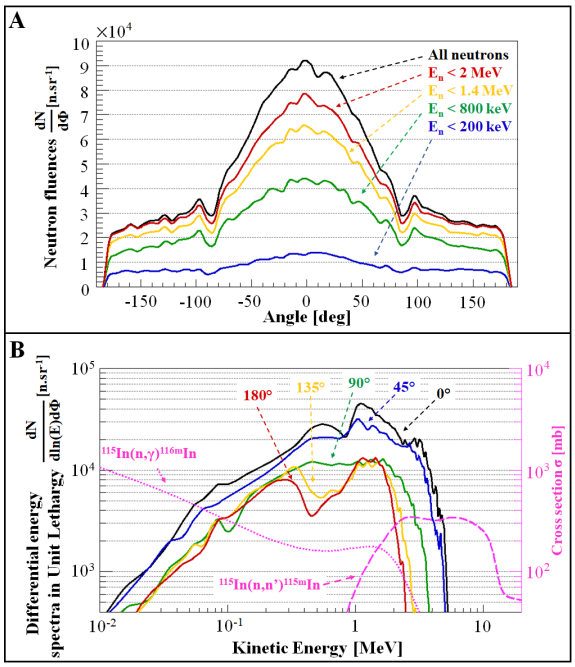

Figure 2. (A) Simulated angular distribution of the neutron emissions recorded in the equatorial plane and passing through the converter center, and (B) differential energy spectra, in unit lethargy, obtained at different angles from Geant4 simulations. Overlaid are the cross sections (in pink) of the ^{115}In(n, fl)^{116m}In and ^{115}In(n, n′)^{115m}In reactions, according to the IRDFF–II [37] library. These are used for the activation simulations.

2. *Monte-Carlo Simulations*

To predict the characteristics of the neutron emissions, Geant4 simulations were made using the averaged proton spectrum shown in Figure 1.B, injected into the LiF converter within a half angle of 21° to reproduce the beam divergence of a TNSA proton beam [38]. These considerations and the use of the ENDF/B-VIII.0 and TENDL-2019 libraries allow to faithfully reproduce the experimental conditions and the nuclear reactions inside the converter.

Figure 2 presents the simulated angular distribution of neutron emissions and the associated neutron spectra obtained at different angles, from 0° to 180°. These simulation results show that more neutrons, with higher energies, are emitted in the forward direction than in the backward direction. This implies that within the converter, not only compound nuclear reactions occur but also direct nuclear reactions, contributing to the distinctive emission anisotropy. However, the large angular distribution of protons induces a smoothed angular distribution of forward-directed neutron emissions and similar neutron spectra between 0° and 45°.

Additional simulations show that the ^{7}Li(p, n)^{7}Be reaction is responsible for all neutron emissions. This is due to a much lower cross section for the ^{19}F(p, n)^{19}Ne reaction and a higher threshold energy of 4 MeV, and to the fact that protons above 4 MeV represent only around 3% of the total number of protons emitted.

Thus, the total number of neutrons calculated by the simulations is 5.44×10^5 neutrons/shot, corresponding to a simulated ^{7}Be activity of 0.082 Bq/shot. The simulations also yields a fluence of up to 9.20×10^4 neutrons/sr/shot at 0° and a mean value of 5.42×10^4 neutrons/sr/shot in the specific solid angle covered by the indium sample ($\sim 2ß$ sr). This value and the corresponding neutron spectrum were then used to perform activation simulations of the indium sample, using MCNP6 with the IRDFF-II library, as it is more suitable for such modeling than the libraries available in Geant4, leading to a ^{115m}In activity of 0.025 Bq/shot and a ^{116m}In activity of 0.274 Bq/shot.

 doi:10.20944/preprints202405.2051.v1

III. Assessment of Neutron Emissions

A. Activation Measurements

A 2×2" NaI gamma spectrometer, shielded by 10-cm-thick lead bricks, was used to experimentally measure the activation of the converter and indium sample. The efficiency calibration of this spectrometer was performed with a ^{152}Eu calibration point source and extrapolated to the geometries of the LiF converter and indium sample using Geant4 simulations and the efficiency transfer method [39,40] based on the Moens concept [41]. This allows to take into account the sample geometry and the self-attenuation effects of gamma-rays on the measurements.

1. Direct Measurement of the LiF Converter

The LiF converter was used during a series of 292 shots to accumulate a measurable ^{7}Be activity. The gamma spectrometry measurement revealed an activity of 0.072 ± 0.009 Bq/shot and, the number of ^{7}Be nuclei being equivalent to the number of neutrons emitted, we can thus infer a total neutron production of $(4.76 \pm 0.62) \times 10^5$ neutrons/shot, which is 12.5% lower, but close, to the value predicted by the Geant4 simulations.

2. Indium Sample

The indium sample was placed behind the LiF converter (see Figure 1.A), during the same series of 292 shots. Both ^{115m}In and ^{116m}In activities were measured by gamma spectrometry, resulting in 7.89 ± 2.47 Bq and 39.56 ± 11.68 Bq, respectively. Considering the almost flat cross section profile of the $^{115}\mathrm{In}(\mathrm{n},\mathrm{n}')^{115\mathrm{m}}\mathrm{In}$ reaction between 2 and 10 MeV (see Figure 2.B), a neutron fluence in this energy range can be evaluated using the following equation:

$$N_\Omega = \frac{A_{\mathrm{mes}}}{\lambda \times n_{\mathrm{shot}}} \times \frac{1}{\bar{\sigma} \times t \times n \times \chi} \times \frac{1}{\Omega} \tag{1}$$

With:

N_Ω, in units of neutrons/sr/shot
A_{mes} , the measured activity (in Bq)
λ, the decay constant (s^{-1})
n_{shot}, number of shots
$\bar{\sigma}$, the average cross section (m^{-2})
t, the sample thickness (m)
n, number density (m^{-3})
χ, the isotope abundance
Ω, the solid angle covered by the sample (sr)

Thus, the ^{115m}In measured activity of 0.013 Bq/shot would correspond to a neutron fluence of $(6.99 \pm 2.19) \times 10^3$ neutrons/sr/shot between 2 and 10 MeV, in the specific solid angle covered by the indium sample, which is very close to the fluence of 6.76×10^3 neutrons/sr/shot predicted by the simulations (and normalized by the ^{7}Be activity measurement) in the same energy range and solid angle. The measurement therefore confirms the proportion of around 1.45% of neutrons above 2 MeV obtained by the simulations.

However, as shown in Table 1, the ^{115m}In simulated activity (0.022 Bq/shot) is much higher than the measured value, which is not consistent with the good agreement between the evaluated and simulated fluences. This is due to an erroneous evaluation of the cross sections of the $^{115}\mathrm{In}(\mathrm{n},\mathrm{n}')^{115\mathrm{m}}\mathrm{In}$ reaction by the IRDFF-II library for neutrons below 2 MeV, resulting in an overestimation of the activity. This was confirmed by an experiment we performed at the AMANDE facility [42] (IRSN, Cadarache) where indium samples were irradiated by monoenergetic neutrons. A comparison between measured and simulated activities revealed an overestimation of the simulated activities, especially for neutrons

 doi:10.20944/preprints202405.2051.v1

between 0.565 and 1.2 MeV. Furthermore, if only neutrons above 2 MeV are considered in the activation simulations, we obtain a ^{115m}In activity of 0.011 Bq/shot, which is more consistent with the measured activity.

The comparison between the measured and simulated ^{116m}In activities is also shown in Table 1. The measured activity is about 4 times lower than expected which means that, considering the cross section distribution of the ^{115}In(n, fl)^{116m}In reaction, the actual low-energy part of the neutron spectrum seems reduced compared to what is predicted by the simulations. In summary, these activation measurements show that fewer neutrons are emitted in the lower energy part of the neutron spectrum, while the proportion of high-energy neutrons (> 2 MeV) is in a good agreement with the simulations.

Table 1. Comparison between the simulated activities, A_{sim}, and the measured activities, A_{meas}, after the last laser shot of the series. ϵ gives the corresponding experimental uncertainties. The simulated activities of the ^{115m}In and ^{116m}In were normalized by the ^{7}Be activity measurement (i.e. by a factor 0.875), to take into account the real production of neutrons.

Reaction	A_{sim}/shot (Bq)	A_{meas}/shot (Bq)	ϵ (%)
^{7}Li(p, n)^{7}Be	0.082	0.072	13.0%
^{116}In(n, fl)^{116m}In	0.240	0.065	29.5%
^{115}In(n, n′)^{115m}In	0.022	0.013	31.3%

B. Bubble Detectors

BDT and BD-PND bubble detectors were also used to characterize the emissions of thermal and fast neutrons, respectively. They were placed outside the target chamber, on the target normal axis (0°), at 60 cm from the LiF converter (see Figure 1.A) and during the same series of 292 laser shots as before.

BDT detectors revealed no bubble, meaning that thermal neutron emissions are negligible, which is consistent with the simulated neutron spectra showing a significant and continuous decrease of the spectrum when the neutron energy decreases.

On the other hand, bubbles were observed in the BD-PND detectors. Considering their energy independent response to neutrons from 200 keV to around 15 MeV, the bubble counting lead to a neutron fluence of $(1.37 \pm 0.15) \times 10^5$ neutrons/sr/shot in this energy range. This neutron fluence is 70% higher than the expected fluence obtained with the Geant4 simulations (normalized by the ^{7}Be activity measurement). The neutron emissions seem therefore more forward-directed than predicted by the simulations.

IV. Discussion

In summary, the use of these three diagnostics (bubble detectors, gamma spectrometry of the LiF converter and of the indium sample) allowed us to conduct the first characterization of neutron emissions generated, using the pitcher-catcher technique, in a high repetition-rate TNSA regime operating at 0.5 Hz, which produces laser-based ion acceleration through the interaction of a high power laser and thin-foil solid targets. The measurement of the ^{7}Be activity produced by the interaction of the protons with the LiF converter led to an estimation of the total neutron production of $(4.76 \pm 0.62) \times 10^5$ neutrons/shot, which is 12.5% lower than the simulation predictions.

The indium sample, measured by gamma spectrometry, presented an activation inducing a neutron fluence of $(6.99 \pm 2.19) \times 10^3$ neutrons/sr/shot between 2 and 10 MeV and fewer emissions of low-energy neutrons compared to the simulations. This observation was confirmed by the absence of bubble inside the BDT detectors. However, the BD-PND detectors showed bubbles from which a neutron fluence of $(1.37 \pm 0.15) \times 10^5$ neutrons/sr/shot was measured, between 200 keV to around 15 MeV, along the normal axis (0°). These quantitative results, summarized in Table 2, suggest a higher

 doi:10.20944/preprints202405.2051.v1

neutron emission than expected in the forward direction and a more sharp energy distribution between a few hundred of keV and 2 MeV.

Table 2. Summary of the measurement of neutron emissions by the three diagnostics used (gamma spectrometry of the LiF converter and of the indium sample, and bubble detectors), showing the simulated Φ_{sim} and measured Φ_{meas} total neutron yield and neutron fluences in different energy ranges. ϵ gives the corresponding experimental uncertainties.

Quantity	Energy range	Φ_{sim}	Φ_{meas}	ϵ (%)
Total neutron yield (n/shot)	All neutrons	5.44×10^5	4.76×10^5	13.0%
Neutron fluences (n/sr/shot)	~ 0.025 eV	0	0	-
	[2-10 MeV]	6.76×10^3	6.99×10^3	31.3%
	[0.2-15 MeV]	8.05×10^4	1.37×10^5	10.9%

The number of neutrons per shot obtained here is about 10^5 lower than what could be obtained using much higher energy lasers [19,43,44], delivering on-target energies of several tens or hundreds of Joules, but which have a very poor repetition rate (with typically one shot per several hours). This points out to the strong nonlinearity of the neutron yield with respect to the input laser energy, but also shows that using laser-based neutrons for the applications demonstrated with these high-energy lasers (thermal neutron radiography or NRS) is not favorable in the conditions demonstrated here, as this would entail accumulating the neutron signal over tens of hours.

Nonetheless, other applications requiring lower neutron fluxes can be considered using the presently demonstrated high-repetition rate, low-yield source. The significant activation of the indium sample measured by gamma spectrometry reveals indeed the possibility of carrying out INAA measurements for the elemental analysis of objects composed of elements whose neutron interaction cross sections are similar or higher to those of indium. This points to a significant advantage of using a laser-based source, since, on the same facility, a range of non-destructive elemental analysis techniques could be deployed, e.g. INAA, but also X-ray Fluorescence (XRF) and Particle-induced X-ray Emission (PIXE) measurements [45]. This is in contrast with conventional accelerators-based sources, where X-ray and neutron sources are produced by different machines.

Fast neutron radiography could also be considered with the neutron flux demonstrated here because, unlike thermal neutron radiography, it does not require to use a moderator to thermalize the neutrons, which usually reduces the neutron flux. Such an application was already performed [46–48] using conventional neutron sources with neutron fluences of about 10^{7-8} neutrons/cm^2. Considering the neutron fluence measured here between 2 and 10 MeV by the indium sample and extrapolating it to the whole spectrum, a total neutron fluence of around 6×10^4 neutrons/cm^2/shot can be inferred. Thus, we estimate that fast neutron radiography could be performed using the ALLS laser by cumulating several hundreds of shots, which represents only a few minutes of irradiation.

Data Availability Statement: The data that support the findings of this study are available from the corresponding author upon reasonable request.

Acknowledgments: The authors would like to acknowledge the staff of the ALLS facility: Joël Maltais, William Lévesque and Mandy Doly for their technical assistance during the experiment, and LaserNetUS for the beamtime provided under proposal K173. This work was supported by the European Research Council (ERC) under the European Union's Horizon 2020 research and innovation program (Grant Agreement No. 787539), by CNRS through the MITI interdisciplinary programs and by IRSN through its exploratory research program, by the National Sciences and Engineering Research Council of Canada (NSERC) (Grant — RGPIN-2023-05459, ALLRP 556340 – 20), Compute Canada (Job: pve-323-ac). The ALLS facility and its ion beamline are funded and supported by the Canadian Foundation for Innovation (CFI), Institute for Quantum Computing, University of Waterloo, INRS, and Ministère de l'Économie, de l'Innovation et de l'Énergie (MEIE) from Québec. This work was supported

 doi:10.20944/preprints202405.2051.v1

by the US Department of Energy Office of Science, Fusion Energy Sciences under Contract No. DE-SC0021246: the LaserNetUS initiative at the Advanced Laser Light Source.

Conflicts of Interest: The authors have no conflicts to disclose.

References

1. Disdier, L.; Garçonnet, J.P.; Malka, G.; Miquel, J.L. Fast Neutron Emission from a High-Energy Ion Beam Produced by a High-Intensity Subpicosecond Laser Pulse. *Phys. Rev. Lett.* **1999**, *82*, 1454.
2. Lancaster et al., K.L. Characterization of Li7(p,n)7Be neutron yields from laser produced ion beams for fast neutron radiography. *Phys. Plasmas* **2004**, *11*, 3404–3408.
3. Alejo, A.; Ahmed, H.; Green, J.; Mirfayzi, S.; Borghesi, M.; Kar, S. Recent advances in laser-driven neutron sources. *Nuovo Cimento C* **2016**, *38C*, 1–7.
4. Alvarez, J.; Fernández-Tobias, J.; Mima, K.; Nakai, S.; Kar, S.; Kato, Y.; Perlado, J. Laser Driven Neutron Sources: Characteristics, Applications and Prospects. *Physics Procedia* **2014**, *60*, 29–38.
5. Pomerantz et al., I. Ultrashort Pulsed Neutron Source. *Physical Review Letters* **2014**, *113*.
6. Higginson et al., D.P. Temporal Narrowing of Neutrons Produced by High-Intensity Short-Pulse Lasers. *Physical Review Letters* **2015**, *115*.
7. Roth et al., M. Bright Laser-Driven Neutron Source Based on the Relativistic Transparency of Solids. *Phys. Rev. Lett.* **2013**, *110*, 044802.
8. Kleinschmidt, A.; Bagnoud, V.; Deppert, O.; Favalli, A.; Frydrych, S.; Hornung, J.; Jahn, D.; Schaumann, G.; Tebartz, A.; Wagner, F.; Wurden, G.; Zielbauer, B.; Roth, M. Intense, directed neutron beams from a laser-driven neutron source at PHELIX. *Phys. Plasmas* **2018**, *25*, 053101.
9. Hornỳ, V.; Chen, S.N.; Davoine, X.; Lelasseux, V.; Gremillet, L.; Fuchs, J. High-flux neutron generation by laser-accelerated ions from single-and double-layer targets. *Sci. Rep.* **2022**, *12*, 19767.
10. Martinez et al., B. Numerical investigation of spallation neutrons generated from petawatt-scale laser-driven proton beams. *Matter Radiat. Extremes* **2021**, *7*, 024401.
11. *https://www.starfireindustries.com/ngen.html*.
12. Comsan, M. Spallation Neutron Sources For Science And Technology. *Proceedings of the eighth Nuclear and Particle Physics Conference (NUPPAC-2011), (p. 287). Egypt* **2011**.
13. Chen, S.N.; Negoita, F.; Spohr, K.; d'Humières, E.; Pomerantz, I.; Fuchs, J. Extreme brightness laser-based neutron pulses as a pathway for investigating nucleosynthesis in the laboratory. *Matter Radiat. Extremes* **2019**, *4*.
14. Horný, V.; Chen, S.N.; Davoine, X.; Gremillet, L.; Fuchs, J. Quantitative feasibility study of sequential neutron captures using intense lasers. *Physical Review C* **2024**, *109*.
15. Brenner et al., C.M. Laser-driven x-ray and neutron source development for industrial applications of plasma accelerators. *Plasma Physics and Controlled Fusion* **2015**, *58*, 014039.
16. Martz Jr, H.E.; Glenn, S. Nuclear techniques to detect explosives. In *Counterterrorist Detection Techniques of Explosives*; Elsevier, 2022; pp. 339–381.
17. Buffler, A. Contraband detection with fast neutrons. *Radiat. Phys. Chem.* **2004**, *71*, 853–861.
18. Buffler, A.; Tickner, J. Detecting contraband using neutrons: challenges and future directions. *Radiation Measurements* **2010**, *45*, 1186–1192.
19. Yogo et al., A. Laser-driven neutron generation realizing single-shot resonance spectroscopy. *Phys. Rev. X* **2023**, *13*, 011011.
20. Kishon, I.; Kleinschmidt, A.; Schanz, V.; Tebartz, A.; Noam, O.; Fernandez, J.; Gautier, D.; Johnson, R.; Shimada, T.; Wurden, G.; Roth, M.; Pomerantz, I. Laser based neutron spectroscopy. *Nuc. Instrum. Meth. A* **2019**, *932*, 27–30.
21. Révay, Z.; Lindstrom, R.M.; Mackey, E.A.; Belgya, T. *Handbook of Nuclear Chemistry: Vol. 3: Chemical Applications of Nuclear Reactions and Radiation*, second ed.; Vol. 3, *Handbook of Nuclear Chemistry*, Springer US, 2010.
22. Smit, Z.; Maróti, B.; Kasztovszky, Z.; Semrov, A.; Kos, R. Analysis of Celtic small silver coins from Slovenia by PIXE and PGAAR. *Archaeological and Anthropological Sciences* **2020**, *12*, 155.
23. Belgya, T. Prompt Gamma Activation Analysis at the Budapest Research Reactor. *Physics Procedia* **2012**, *31*, 99–109.

 doi:10.20944/preprints202405.2051.v1

24. Knight, B.M.; Gautam, C.M.; Stoner, C.R.; Egner, B.V.; Smith, J.R.; Orban, C.M.; Manfredi, J.J.; Frische, K.D.; Dexter, M.L.; Chowdhury, E.A.; Patnaik, A.K. Detailed characterization of kHz-rate laser-driven fusion at a thin liquid sheet with a neutron detection suite. *High Power Laser Science and Engineering* **2023**, *12*. doi:10.1017/hpl.2023.84.
25. Catrix, E.; Boivin, F.; Langlois, K.; Vallières, S.; Boynukara, C.Y.; Fourmaux, S.; Antici, P. Stable high repetition-rate laser-driven proton beam production for multidisciplinary applications on the Advanced Laser Light Source ion beamline. *Review of Scientific Instruments* **2023**, *94*, 103003.
26. Wilks, S.C.; Langdon, A.B.; Cowan, T.E.; Roth, M.; Singh, M.; Hatchett, S.; Key, M.H.; Pennington, D.; MacKinnon, A.; Snavely, R.A. Energetic proton generation in ultra-intense laser–solid interactions. *Phys. Plasmas* **2001**, *8*, 542–549.
27. Snavely et al., R.A. Intense High-Energy Proton Beams from Petawatt-Laser Irradiation of Solids. *Phys. Rev. Lett.* **2000**, *85*, 2945–2948.
28. Romagnani, L.; Fuchs, J.; Borghesi, M.; Antici, P.; Audebert, P.; Ceccherini, F.; Cowan, T.; Grismayer, T.; Kar, S.; Macchi, A.; Mora, P.; Pretzler, G.; Schiavi, A.; Toncian, T.; Willi, O. Dynamics of Electric Fields Driving the Laser Acceleration of Multi-MeV Protons. *Phys. Rev. Lett.* **2005**, *95*, 195001.
29. Agostinelli et al., S. Geant4—a simulation toolkit. *Nuc. Instrum. Meth. A* **2003**, *506*, 250–303.
30. Thompson, W.L. MCNP, a general Monte Carlo code for neutron and photon transport: a summary **1979**.
31. Vallières, S.; Salvadori, M.; Puyuelo-Valdes, P.; Payeur, S.; Fourmaux, S.; Consoli, F.; Verona, C.; d'Humières, E.; Chicoine, M.; Roorda, S.; Schiettekatte, F.; Antici, P. Thomson parabola and time-of-flight detector cross-calibration methodology on the ALLS 100 TW laser-driven ion acceleration beamline. *Review of Scientific Instruments* **2020**, *91*, 103303.
32. Brown, D.A.; Chadwick, M.; Capote, R.; Kahler, A.; Trkov, A.; Herman, M.; Sonzogni, A.; Danon, Y.; Carlson, A.; Dunn, M.; others. ENDF/B-VIII.0: the 8th major release of the nuclear reaction data library with CIELO-project cross sections, new standards and thermal scattering data. *Nuclear Data Sheets* **2018**, *148*, 1–142.
33. Koning, A.; Rochman, D.; Sublet, J.C.; Dzysiuk, N.; Fleming, M.; Van der Marck, S. TENDL: complete nuclear data library for innovative nuclear science and technology. *Nuclear Data Sheets* **2019**, *155*, 1–55.
34. Higginson et al., D.P. Global Characterization of a Laser-Generated Neutron Source, 2023.
35. Lelièvre et al., R. A Comprehensive Characterization of the Neutron Fields Produced by the APOLLON Petawatt Laser. *arXiv* **2023**, p. arXiv.2311.12653.
36. Ing, H.; Noulty, R.; McLean, T. Bubble detectors—a maturing technology. *Radiation measurements* **1997**, *27*, 1–11.
37. Trkov et al., A. IRDFF-II: A New Neutron Metrology Library. *Nuclear Data Sheets* **2020**, *163*, 1–108.
38. Mancic et al., A. Isochoric heating of solids by laser-accelerated protons: Experimental characterization and self-consistent hydrodynamic modeling. *High Energy Density Physics* **2010**, *6*, 21–28.
39. Vidmar, T. EFFTRAN—A Monte Carlo efficiency transfer code for gamma-ray spectrometry. *Nuc. Instrume. Meth. A.* **2005**, *550*, 603–608.
40. Chagren, S.; Tekaya, M.B.; Reguigui, N.; Gharbi, F. Efficiency transfer using the GEANT4 code of CERN for HPGe gamma spectrometry. *Applied Radiation and Isotopes* **2016**, *107*, 359–365.
41. Moens, L.; De Donder, J.; Xi-Lei, L.; De Corte, F.; De Wispelaere, A.; Simonits, A.; Hoste, J. Calculation of the absolute peak efficiency of gamma-ray detectors for different counting geometries. *Nuc. Instrum. Meth.* **1981**, *187*, 451–472.
42. Gressier, V.; Guerre-Chaley, J.F.; Lacoste, V.; Lebreton, L.; Pelcot, G.; Pochat, J.L.; Bolognese-Milstajn, T.; Champion, D. AMANDE: a new facility for monoenergetic neutron fields production between 2 keV and 20 MeV. *Radiation Protection Dosimetry* **2004**, *110*, 49–52.
43. Yogo et al., A. Single shot radiography by a bright source of laser-driven thermal neutrons and x-rays. *Appl. Phys. Express* **2021**, *14*, 106001.
44. Zimmer et al., M. Demonstration of non-destructive and isotope-sensitive material analysis using a short-pulsed laser-driven epi-thermal neutron source. *Nature Communications* **2022**, *13*, 1173.
45. Puyuelo-Valdes, P.; Vallières, S.; Salvadori, M.; Fourmaux, S.; Payeur, S.; Kieffer, J.C.; Hannachi, F.; Antici, P. Combined laser-based X-ray fluorescence and particle-induced X-ray emission for versatile multi-element analysis. *Sci. Rep.* **2021**, *11*, 9998.

 doi:10.20944/preprints202405.2051.v1

46. Williams, D.L.; Brown, C.M.; Tong, D.; Sulyman, A.; Gary, C.K. A Fast Neutron Radiography System Using a High Yield Portable DT Neutron Source. *Journal of Imaging* **2020**, *6*.
47. Zboray, R.; Adams, R.; Kis, Z. Scintillator screen development for fast neutron radiography and tomography and its application at the beamline of the 10 MW BNC research reactor. *Applied Radiation and Isotopes* **2018**, *140*, 215–223.
48. Bergaoui, K.; Reguigui, N.; Gary, C.K.; Cremer, J.T.; Vainionpaa, J.H.; Piestrup, M.A. Design, testing and optimization of a neutron radiography system based on a Deuterium–Deuterium (D–D) neutron generator. *J. Radioanal. Nucl. Chem.* **2014**, *299*, 41–51.